Effect of hydrogenation on type II silicon clathrate films

Maxime Hanauer, Anil Kumar Bharwal, Yongfeng Tong, Brahim Aissa, Charif Tamin, Stéphane Roques, Dominique Muller, Céline Chevalier, Aziz Dinia, Abdelilah Slaoui, et al.

Effect of hydrogenation on type II silicon clathrate films

Journal of Physics: Energy

PAPER

Effect of hydrogenation on type II silicon clathrate films

Maxime Hanauer[1,2], **Anil Kumar Bharwal**[1,*], **Yongfeng Tong**[3], **Brahim Aissa**[3], **Charif Tamin**[4], **Jérémy Bartringer**[1], **Stéphane Roques**[1], **Dominique Muller**[1], **Céline Chevalier**[4], **Aziz Dinia**[2], **Abdelilah Slaoui**[1] **and Thomas Fix**[1,*]

[1] ICube Laboratory, University of Strasbourg and CNRS, 67037 Strasbourg, France
[2] IPCMS Laboratory, University of Strasbourg and CNRS, 67037 Strasbourg, France
[3] Qatar Environment and Energy Research Institute (QEERI), Hamad Bin Khalifa University (HBKU), 34110 Education City, Doha, Qatar
[4] CNRS, Ecole Centrale de Lyon, INSA Lyon, Université Claude Bernard Lyon 1, CPE Lyon, INL, UMR5270, 69100 Villeurbanne, France
* Authors to whom any correspondence should be addressed.

E-mail: anilbharwal@gmail.com and tfix@unistra.fr

Keywords: silicon clathrate films, plasma hydrogenation, ToF-SIMS, chemical depth profiling, ERDA, energy levels

Supplementary material for this article is available online

OPEN ACCESS

RECEIVED
10 July 2025

REVISED
19 August 2025

ACCEPTED FOR PUBLICATION
4 September 2025

PUBLISHED
16 September 2025

Abstract

In this study we investigate for the first time the effect of hydrogenation on the properties of type II silicon clathrate films (SiCL). These clathrates are an alternative form of silicon based on a cage structure. It can be either emptied or filled with sodium atoms, leading to a metallic or semiconducting behavior with a tunable direct bandgap of 1.6–1.8 eV. There are a wide range of potential applications for such materials such as in electronics, optoelectronics, photovoltaics, batteries, spintronics or hydrogen (H) storage. However, the role of H in such materials remains largely unexplored and is not well understood experimentally. In this work, we hydrogenate the clathrates films using a H plasma with a substrate temperature of 400 °C. We evaluate the H content in the films by Time-of-Flight Secondary Ion Mass Spectrometry and Elastic Recoil Detection Analysis. The latter indicates a $SiH_{0.006}$ molar concentration before and $SiH_{0.070}$ after hydrogenation. Such a H content within the SiCL films is too low for practical hydrogen storage applications. Nevertheless, the incorporated H plays the role of dopant, leading to a reduction in the work function by around 0.3 eV. This demonstrates that even a modest hydrogen uptake can significantly enhance the electronic properties of silicon clathrates.

1. Introduction

Cage-like structured materials, such as C_{60} [1], metal–organic frameworks [2] and clathrates [3, 4], are attracting much interest in various scientific fields due to their potential for energy applications. Among them, silicon clathrate (SiCL), an alternative form of Si consisting in nanocages of various sizes, has been under development and study intensively. Discovered in the bulk in 1965 [5], practical applications have only emerged more recently, following advances in the fabrication of SiCL in thin films form [4, 6, 7]. There are two main types of SiCL: Type-I (Na_8Si_{46}) exhibiting a metallic behavior [8] and Type-II (Na_xSi_{136}) presenting varying properties depending on the sodium concentration, from semiconductor to metallic [9–13]. The ability to tune the properties through guest atom concentration, combined with the presence of a direct bandgap in Type-II SiCL, makes these materials particularly promising for optoelectronic applications, as potential alternative to well-known diamond silicon (d-Si) [14, 15].

The interplay between hydrogen (H) and d-Si has been well studied, particularly in the context of hydrogenated amorphous silicon (a-Si:H), where H is especially known to passivate surface dangling bonds [16–18]. This passivation can induce a shift of the Fermi level (E_F) due to the dopant character of H [19–21]. Nevertheless, the influence of H on SiCL remains experimentally unexplored, despite expectations that the

cage structure of SiCL and the defects observed present many dangling bonds. Moreover, H is expected to fill the cages, as performed with alkali atoms [6, 22, 23]. Thus silicon clathrates have been envisaged for H storage, but key merit factors to evaluate the applicability of such a concept are still lacking [24]. Within the frame of research on H for energy applications, the US Department of Energy (DOE) has defined ambitious targets for H storage materials: 5.5 wt% gravimetric H capacity by 2025, and 6.5 wt% as an ultimate goal for light-duty fuel cell vehicles [25–27].

In this study, we present the hydrogenation of Type-II SiCL films thanks to a H plasma. H content and distribution are evaluated using Elastic Recoil Detection Analysis (ERDA) and Time-of-Flight Secondary Ion Mass Spectroscopy (ToF-SIMS) techniques respectively, and electronic energy levels are then determined using the Kelvin probe (KP) method. Different types of samples were hydrogenated. In particular, we worked both on Na-filled and Na-free cages thanks to our recent advances in SiCL iodine treatment to remove sodium from the cages [4, 11].

2. Experimental section

2.1. Materials

Type-II SiCL (Na_xSi_{136}) films were previously synthesized using p-type silicon wafers from BTelectronics (thickness 525 $\pm$ 25 μm, resistivity = 1–5 Ω cm following the procedure described by Fix *et al* [4]. Post-fabrication treatments were applied as detailed in the references to enhance the film density and overall quality (thermal-pressing) [4, 28] and also to reduce the sodium content (iodine treatment), thereby enhancing the semiconducting properties [11, 13]. The various sample names and their corresponding surface treatments are presented in the table 1.

2.2. Plasma hydrogenation treatment of type II silicon clathrate films

Hydrogenation experiments were performed using a microwave (MW)—electron cyclotron resonance (ECR) plasma system from Roth and Rau commonly used for PECVD. A schematic of this setup is shown elsewhere [29]. In this system, H_2 gas is excited by a 2.45 GHz MW in a resonant chamber, where a magnetic field is applied to maintain the ECR condition. The gas pressure of the plasma is maintained at 0.01 Pa, with a H_2 flow of 30 sccm. The hydrogenation duration is 60 min. The MW plasma power and substrate temperature are maintained at 500 W and 400 °C, respectively. Throughout the process, both the incident MW power and the reflected power are monitored, with minimal reflected power observed (<5%), indicating stable plasma conditions. The sample is then removed from the reactor right after the plasma extinction to provoke rapid quenching of the sample, thereby preserving the hydrogenation state. The experimental conditions used in this study have been optimized for the hydrogenation of diamond silicon [29]. Moreover, the chosen temperature is suitable for SiCL films, as it is the one needed for the second synthesis step.

2.3. Characterization techniques

X-ray diffraction (XRD) analysis was performed using a Bruker D8 DISCOVER device with Cu $K_{\alpha 1}$ radiation (wavelength of 0.154 059 nm) to characterize the structural properties, along with a JOBIN YVON LabRam Aramis system using a 532 nm laser for both Raman spectroscopy and photoluminescence measurements at 293 K. The in-depth chemical composition of our films was probed using Time-of-Flight Secondary Ion Mass Spectroscopy (ToF-SIMS) with an IONTOF^{TM} instrument equipped with a primary Bi^+ beam of 30 kV and a sputter Cs^+ beam of 2 kV. In-depth H quantifications were performed using ERDA with a 4 MV Van de Graaff accelerator (KN4000 model built by HVEE), using a He^+ beam of 2750 keV, with the detector at 10° angle with respect to the incident beam direction. The calibration was done using hydrogenated p-type Si substrates from BTelectronics (thickness 525 $\pm$ 25 μm, resistivity = 1–5 Ω cm) under the same process conditions used for SiCL films hydrogenation. Results, provided in Supplementary Information (figures S1 and S2), indicate standard hydrogenation behavior of diamond-like silicon (d-Si), with surface H concentration reaching up to $SiH_{0.45}$. Both ERDA and ToF-SIMS exhibited consistent features, with the presence of an intense and narrow H peak at the surface, indicating shallow implantation and surface accumulation. A multifunctional system (APS03, KP Technology) was used for KP, and Ambient pressure Photoemission Spectroscopy (APS) measurements, without moving the sample position between measurements, allowing accurate determination of the sample's energy levels. The KP and APS techniques have been previously described in detail in [30].

Table 1. Sample designation and associated surface treatments. More information on the surface treatments can be found in supporting information table S1.

Sample Name	Thermal pressing *(Film enhancement)*	Iodine *(Na removal)*	Hydrogenated
A (As-grown)	—	—	—
B	—	—	✓
C	—	✓	✓
D	✓	✓	—
E	✓	✓	✓

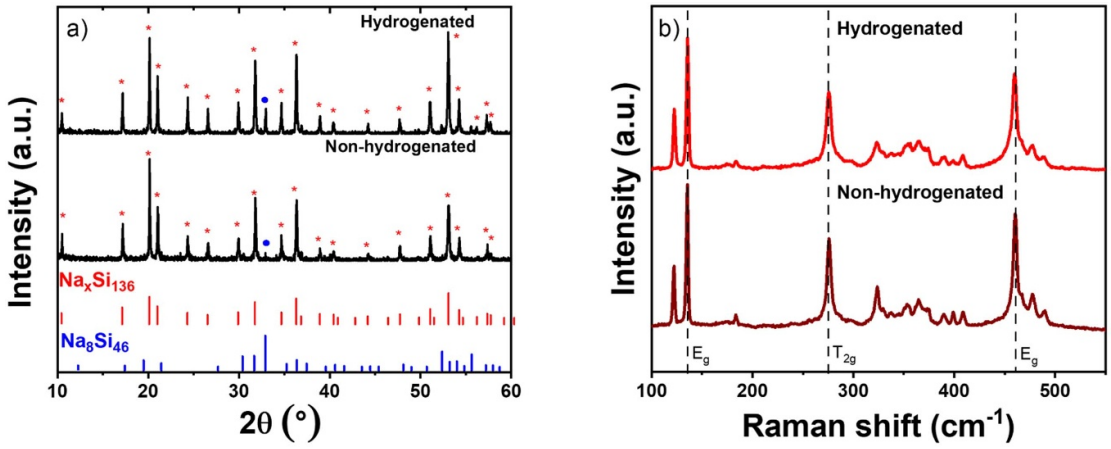

Figure 1. (a) Room temperature θ–2θ XRD patterns and (b) micro-Raman scattering spectra of Na_xSi_{136} films before and after hydrogenation. In (a) peaks are identified by a blue circle for type I and a red star for type II clathrates.

3. Results and discussion

Following the hydrogenation treatment, XRD and micro-Raman were first used to verify the non-degradation of the clathrates phase post-treatment. Subsequently, the H content and distribution were evaluated using ERDA and ToF-SIMS techniques. ToF-SIMS was also helpful to probe possible chemical modifications in the film. Finally, the influence on the energy levels of the samples was assessed through KP, APS and PL techniques.

3.1. Structural characterization of hydrogenated Na_xSi_{136} films

First, room-temperature θ–2θ XRD and micro-Raman spectroscopy were performed on the hydrogenated films to confirm the Type-II phase (figure 1(a)). The XRD patterns display all expected peaks related to the ICDD sheet number 00-018-1244 with only minor traces of type-I phase observed (e.g. at $2\theta = 32.9°$). After hydrogenation, the patterns remain quite similar, confirming the non- degradation of the structure. As shown previously, the intensity ratio of some Type-II peaks can be related to the Na occupancy in the cages [11, 13]. Such ratio changes are observed after H treatment (e.g., at 21° and 53 °), which could imply a small modification of the Na occupancy between 0.1 and 23 Na per 136 Si [11]. The Na content will be further evaluated by ToF-SIMS. Raman spectroscopy was also used to confirm the non-degradation of our structure upon plasma hydrogenation. The resulting spectra are presented in figure 1(b), where the principal peaks are aligned with their known vibrational modes [30, 31]. The Raman spectra confirm the absence of clathrate degradation in the hydrogenated films, as also observed by XRD.

3.2. Hydrogen probing in films

After confirming the preservation of the clathrate phase, the H content was determined by ToF-SIMS and ERDA measurements. ToF-SIMS was used in a semi-quantitative manner (i.e. without intensity calibration), allowing comparison of elemental profiles based on signal intensity. For quantitative H analysis, ERDA was employed.

ToF-SIMS depth profiles, allows the in-depth assessment of the number of Si, H and Na atoms (i.e. intensity changes) present within the SiCL films before and after different processes. O that may originate from a native oxide layer, I from the I_2 treatment and C that may from adventitious C contamination [32] were also probed. In fact, all these elements are found in our samples. The sputter time

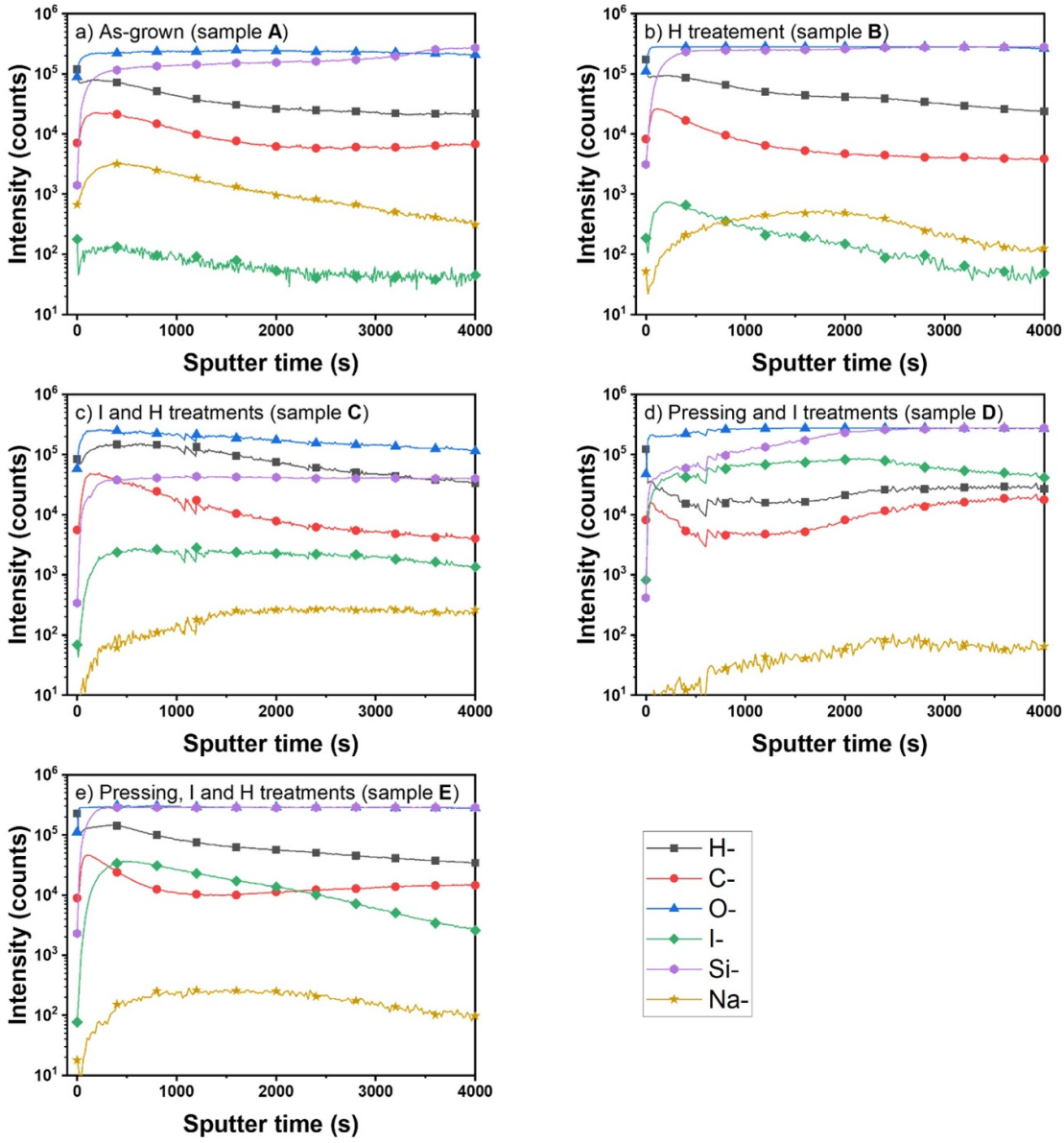

Figure 2. ToF-SIMS depth profiles of electronegative elements in Na_xSi_{136} films with different surface treatments.

of 4000 s represents an estimated depth of about 2 μm in the SiCL film. We report as follow the results of the five different types of clathrate sample from (table 1).

Figure 2(a) exhibits the SIMS profile of as-grown SiCL film (**A**). As this film received no I treatment, any I is likely due to cross-contamination. The Si signal is constant with sputtering time, which is expected for a uniform composition film, alongside with O. In this case, the O profile is not characteristic of a native oxide layer; otherwise, a strong surface peak would appear at the start of the sputtering and then decrease. C and H elements are present and decrease steadily throughout the film depth, showing similar profiles. These elements may originate from hydrocarbon traces introduced during the processing of sodium that is placed in cyclohexane to prevent oxidation before the evaporation to form the Na_4Si_4 precursors. Na is present along all the clathrate film thickness but decreases with depth, which can be explained by Na migration and expulsion from the film when annealing the Na_4Si_4 precursor.

Figure 2(b) presents the distribution of the elements within the SiCL film after plasma hydrogenation (**B**). The C and H profiles do not strictly follow the same trend vs sputter time as opposed to sample **A**, which illustrates that the H in this case may not originate from hydrocarbon contamination. Conversely, the Na intensity decreases and its profile is no longer linear. Indeed, as hydrogenation occurs at 400 °C, Na atoms may have desorbed and diffused towards the surface, explaining the slight changes also observed in previous XRD spectra. The I signal is present as well, with a prominent surface peak and a decreasing signal in depth, most likely due to contamination from other samples.

Figure 2(c) shows data of the as-grown sample treated first with I to remove Na and then hydrogenated (**C**). The C and H signals again do not follow the same profile vs sputter time, as depicted in sample **B**, which reinforce the confirmation of effective hydrogenation. Notably, the H intensity exceeds 10^5 counts, higher than for sample A and B, without I treatment. I is homogeneously distributed in the film, originating from the Na removal treatment.

Figure 2(d) displays elemental profiles for a mechanically pressed SiCL sample, and then treated with iodine but non hydrogenated (**D**). The H profile closely follows that of the carbon, likely reflecting adventitious carbon. The significant reduction of sodium is evident due to iodine treatment, confirmed by a stable iodine signal intensity above 10^4 counts throughout the film.

The SIMS profile of the pressed, I treated and hydrogenated film (**E**) is shown in figure 2(e). It reveals an effective H incorporation, with C and H signals clearly differentiated, like in the other hydrogenated films. Yet, Na removal is less effective than in the non-hydrogenated pressed sample (**D**), with Na intensity above 10^2 counts. I is mostly present near the surface, with intensity decreasing with sputtering depth. Since both pressed samples originate from the same synthesized clathrates and underwent identical iodine treatment, this suggests that hydrogenation promotes sodium diffusion from deeper within the film. It should be noted that I treatment is a surface-level process, so the Na atoms located at the Si/SiCL interface may remain unreacted and unreleased. Moreover, the film is 30 μm thick, while the ToF-SIMS analysis probed less than 2 μm of depth, Na in the bulk may not be probed by this technique.

In summary, hydrogenation appears effective across the different post-treatments investigated. However, H incorporation is not the only effect of the applied plasma process. Thermal annealing plays a significant role, inducing Na diffusion within the film. Moreover, our results reveal notable I contamination originating from the Na removal treatment. Lastly, C contamination is present even in non-hydrogenated samples, and can be likely attributed to contamination from the cyclohexane that prevents oxidation of Na.

The ToF-SIMS results reported above have confirmed the presence of H in the films. Subsequently, ERDA was then employed to quantify the H content, while probing a depth of approximately 1 μm. However, due to the grazing incidence beam used in ERDA and the high surface roughness of non-pressed films ($>$ 10 μm, as reported by Fix *et al* [4]), analysis of these samples is challenging. Therefore, only ERDA data from thermally pressed films before and after hydrogenation (samples **D** and **E** respectively) are displayed in figure 3. Consistent with the ToF-SIMS analysis, H is present in the as-grown film but its amount increases significantly after hydrogenation. Unlike the sharp, surface-localized H peak typically observed in hydrogenated silicon wafer (see SI.2), SiCL exhibits in-depth incorporation, evidenced by a non-Gaussian profile. The experimental H profile was simulated using the SAM software, presented in detail by Stoquert *et al* in [33], which generates diffusion profiles owing to an erfc(x) function after a background noise correction (figure S3). The simulation estimates a H concentration of $3.0{\cdot}10^{16}$ H cm^{-2} in the untreated pressed film, increasing to $1.2{\cdot}10^{17}$ H cm^{-2} after hydrogenation, both values integrated over the first 1 μm of depth. This corresponds to film compositions of approximately $SiH_{0.006}$ and $SiH_{0.07}$, before and after hydrogenation respectively. Assuming the type-II SiCL structure consists of 16 Si_{20} and 8 Si_{28} face-sharing cages per unit cell (noted $[5^{12}]_{16}[5^{12}6^4]_8$ [8]); the maximum H content per cage was estimated. This yields about 0.14 H per cage (0.12 H per Si_{20} cage and 0.17 H per Si_{28} cage) for the non-hydrogenated pressed film, to be compared to 1.59 H per cage (1.4 H per Si_{20} cage and 1.96 H perSi_{28} cage) for the hydrogenated pressed film. This results in a gravimetric quantity of 0.25 wt%, which remains significantly below the 5.5 wt% target set by the DOE for H storage in a solid matrix.

To summarize, ToF-SIMS and ERDA analysis have demonstrated a substantial tenfold increase in the H content of the films following the H plasma treatment, as corroborated with SAM software for the pressed samples. While ToF-SIMS analysis provided comparative elemental profiling across the different samples, it does not allow quantitative measurement and may introduce slight alterations due to the sputtering process. Conversely, ERDA allows a more quantitative measure of H concentration; though, the simulations may not fully account for the influence of Na and I atoms, which could affect accuracy.

3.3. Energy levels analysis

The analyses presented above confirm the effective incorporation of H into the plasma-treated SiCL films. The subsequent question concerns the impact of H incorporation on the semiconducting properties of SiCL. Therefore, we investigated through the energy levels before and after hydrogenation using a combination of techniques, (KP, APS, PL) to extract the work function (WF), ionization energy (IE) and bandgap respectively (table S2 and figures S4 and S5).

The deduced energy levels, in reference to the vacuum energy, of the non-pressed films are shown in figure 4. The as-grown sample (**A**) exhibits n-type behavior, with a bandgap of approximately 1.7 eV and an energy difference between the conduction band (CB) and the Fermi level (E_F) of 0.5 eV. Following hydrogenation, no significant change in the bandgap is observed compared to the as-grown sample,

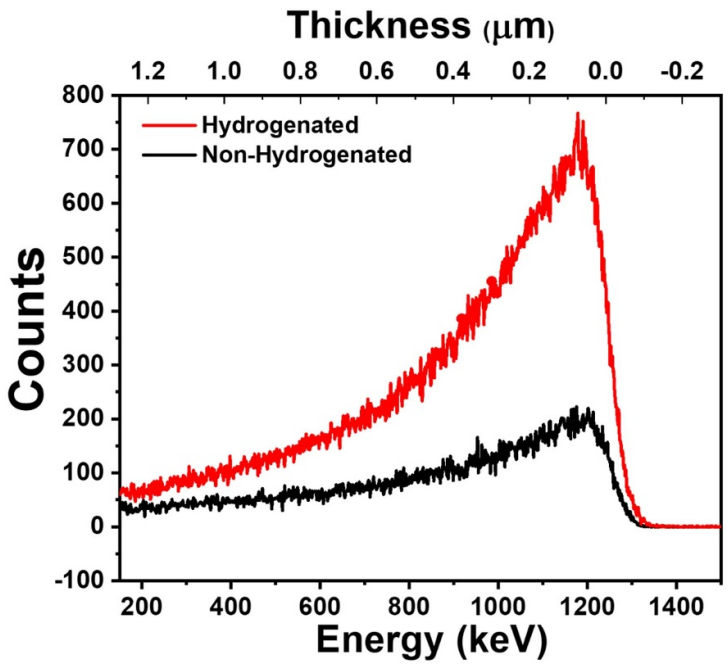

Figure 3. Experimental ERDA profiles of pressed and iodine treated films (**D** and **E**).

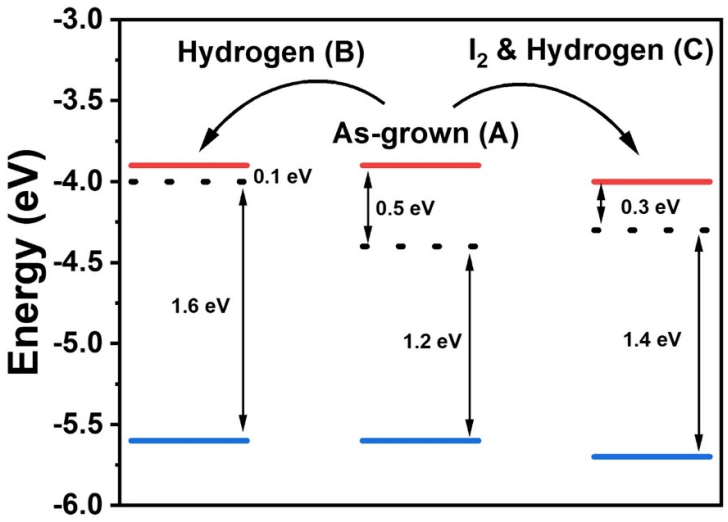

Figure 4. Energy level diagrams of non-pressed Na_xSi_{136} films with different treatments, considering the vacuum level at 0 eV.

regardless of whether I treatment was applied prior to hydrogenation. However, a slight shift in IE (0.1 eV) is noted upon I treatment (**C**). This shift is not very large compared to the uncertainty of IE determination of ±0.05 eV. However, the most pronounced change is observed in the WF, showing E_F going towards the CB after hydrogenation (samples **B** and **C**). This effect is more pronounced in samples not subjected to I treatment (**B**). This behavior is consistent with prior observations indicating that Na removal shifts E_F toward the VB [13]. Therefore, as sample **C** has less Na, its E_F is lower than in **B**, and so it counteracts the influence of H. This suggests that H acts as an electron donor as in the case of Na, leading to a more n-type character with increased H concentration. It is to be noted that this effect solely originates from H incorporation, as thermal treatment at 400 °C would induce a Na diffusion out of the film. However, this diffusion is too slow to induce any modification of the energy levels. Additionally, Tamin *et al* have observed a thin oxidized layer on the SiCL surface by XPS [15], which merely induces any energy band modification. Yet, the hydrogenation induces a WF shift that would more likely originate from a bulk doping, with a carrier density increase in the energy levels, than a surface termination modification.

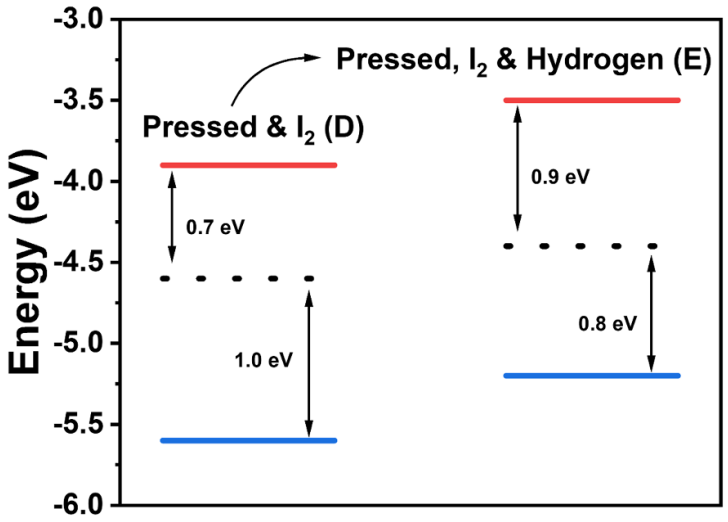

Figure 5. Energy level diagrams of pressed and iodine treated Na_xSi_{136} films, considering the vacuum level at 0 eV.

Sample **D** (pressed and iodine treatment) has a higher WF than the previous sample **A** (as-grown) due to a lower Na content as evidenced by ToF-SIMS. Indeed, according to Bharwal *et al* [13], a decreased Na concentration in SiCL tends to promote more intrinsic behavior, where the E_F goes down away from the CB. Hydrogenation of the pressed and iodine treated sample (from **D** to **E**) induces a noticeable shift of 0.4 eV of both the CB and VB toward the vacuum level energy, as shown in figure 5. Additionally, the WF shifts by about 0.2 eV toward the center of the bandgap, resulting in a more intrinsic-like semiconducting behavior. This shift is unexpected because sample **E** compared to sample **D** has more H and more Na according to ToF-SIMS, so that the E_F should be higher. Therefore, it seems that the fact that the CB has shifted up by 0.4 eV in sample E renders the H and Na dopants less effective. To fully understand these complex results, DFT calculations may be welcome in a future work.

4. Conclusion

In summary, we have successfully incorporated H atoms into Na_xSi_{136} films via plasma hydrogenation treatment. By combining ToF-SIMS and ERDA analyses, we demonstrated the evolution of the chemical composition across different film types, with H concentration increasing in pressed films by a factor of 10 compared to a non-hydrogenated sample. Moreover, the combination of APS, KP and PL measurements revealed a shift in the Fermi level induced by the plasma process, with H acting as n-type dopant in non-pressed films. This study confirms the feasibility of hydrogenating Type-II SiCL films, although further studies may be welcome in the future. In particular, combination with other post-deposition treatments such reactive ion etching of the surface can be envisaged [28], as well as testing other hydrogenation procedures and conditions. However, the H incorporation level achieved with the current protocol remains, yet, insufficient for H storage applications, falling well below the DOE target. As there is currently no clear understanding of how the conditions can affect the hydrogenation, further experimental work is necessary to understand and optimize the H incorporation in SiCL films. Alternative hydrogenation conditions, such as different processing temperature, duration and gas composition, have to be explored.

Data availability statement

All data that support the findings of this study are included within the article (and any supplementary files).

Supplementary data available at https://doi.org/10.1088/2515-7655/ae0368/data1.

Acknowledgment

This work was supported by ANR Exosil-Exotic Silicon: Silicon clathrate films (project-ANR-22-CE50-0025).

The authors thank the HBKU Core Labs for ToF-SIMS measurements, the C^3Fab platform, ACACIA pole for ERDA measurements and the XRD platform of the IPCMS laboratory.

Author contributions

Maxime Hanauer 0009-0002-0334-2172
Conceptualization (equal), Investigation (lead), Methodology (equal), Writing – original draft (lead), Writing – review & editing (equal)

Anil Kumar Bharwal 0000-0002-7350-1637
Investigation (equal), Supervision (equal), Writing – review & editing (equal)

Yongfeng Tong
Investigation (equal), Methodology (equal), Writing – review & editing (equal)

Brahim Aissa
Investigation (equal), Methodology (equal), Writing – review & editing (equal)

Charif Tamin
Investigation (equal)

Jérémy Bartringer
Investigation (equal)

Stéphane Roques 0009-0004-9729-3707
Investigation (equal)

Dominique Muller
Investigation (equal), Methodology (equal), Writing – review & editing (equal)

Céline Chevalier
Investigation (equal)

Aziz Dinia
Conceptualization (equal), Project administration (equal), Supervision (equal), Writing – review & editing (equal)

Abdelilah Slaoui
Conceptualization (equal), Project administration (equal), Supervision (equal), Writing – review & editing (equal)

Thomas Fix 0000-0002-1531-725X
Conceptualization (equal), Project administration (lead), Supervision (lead), Writing – review & editing (equal)

Appendix. Supporting information

Sample name and post-treatments; KP systems output values; ToF-SIMS depth profile of Si:H wafer; ERDA profile of Si:H wafer and associated simulation; Background noise canceled spectra; IE and fitting spectra; PL spectra examples

References

[1] Nakamura Y, Kagawa F, Kasai K, Mera Y and Maeda K 2004 Nonthermal decomposition of C60 polymers induced by tunneling electron injection *Appl. Phys. Lett.* **85** 5242–4
[2] Qiu T, Liang Z, Guo W, Tabassum H, Gao S and Zou R 2020 Metal–organic framework-based materials for energy conversion and storage *ACS Energy Lett.* **5** 520–32
[3] Mano S, Onimaru T, Yamanaka S and Takabatake T 2011 Off-center rattling and thermoelectric properties of type-II clathrate $(K, Ba)_{24}(Ga, Sn)_{136}$ single crystals *Phys. Rev. B* **84** 214101
[4] Fix T, Vollondat R, Ameur A, Roques S, Rehspringer J-L, Chevalier C, Muller D and Slaoui A 2020 Silicon clathrate films for photovoltaic applications *J. Phys. Chem. C* **124** 14972–7
[5] Kasper J S, Hagenmuller P, Pouchard M and Cros C 1965 Clathrate structure of silicon Na_8Si_{46} and Na_xSi_{136} ($x < 11$) *Science* **150** 1713–4
[6] Warrier P and Koh C A 2016 Silicon clathrates for lithium ion batteries: a perspective *Appl. Phys. Rev.* **3** 040805
[7] Al Maksoud W, Bacha R U S, Pixius J, Viswanathan M, Vaishnav Y, Rai R K, Hedhili M N, Wang Q and Kobayashi Y 2024 Silicon clathrate-supported catalysts with low work functions for ammonia synthesis *Adv. Mater.* **36** 2406944
[8] Vollondat R, Roques S, Chevalier C, Bartringer J, Rehspringer J-L, Slaoui A and Fix T 2022 Synthesis and characterization of silicon clathrates of type I Na_8Si_{46} and type II $NaxSi_{136}$ by thermal decomposition *J. Alloys Compd.* **903** 163967
[9] Stefanoski S, Malliakas C D, Kanatzidis M G and Nolas G S 2012 Synthesis and structural characterization of $NaxSi_{136}$ ($0 < x \leqslant 24$) single crystals and low-temperature transport of polycrystalline specimens *Inorg. Chem.* **51** 8686–92

[10] Dopilka A, Weller J M, Ovchinnikov A, Childs A, Bobev S, Peng X and Chan C K 2021 Structural origin of reversible Li insertion in guest-free, Type-II silicon clathrates *Adv. Energy Sustain. Res.* **2** 2000114
[11] Vollondat R, Stoeffler D, Preziosi D, Roques S, Slaoui A and Fix T 2023 Tunability of silicon clathrate film properties by controlled guest-occupation of their cages *J. Chem. Phys.* **158** 164709
[12] Xue D, Deng Y and Myles C W 2024 Probing the mechanism of guest–framework bonding interactions through a first-principles study on the structural and electronic properties of type-II clathrate AxSi136 (A = Na, K, Rb; $0 \leqslant x \leqslant 24$) under pressure *RSC Adv.* **14** 20220–9
[13] Bharwal A K, Vollondat R, Tamin C, Roques S, Bartringer J, Stoeffler D, Chevalier C, Dinia A, Slaoui A and Fix T 2024 Influence of sodium concentration on the optoelectronic properties of silicon clathrate films *ACS Appl. Energy Mater.* **7** 8554–61
[14] Kume T *et al* 2016 Thin film of guest-free type-II silicon clathrate on Si(111) wafer *Thin Solid Films* **609** 30–34
[15] Tamin C, Bharwal A K, Chevalier C, Fave A, Fourmond E, Roques S, Dinia A, Slaoui A and Fix T 2025 Exploring the potential of silicon clathrate films with NiOx-based selective contacts for optoelectronic devices *Adv. Mater. Interfaces* **12** e00301
[16] Hanoka J I 1986 Hydrogen Passivation of Polycrystalline Silicon *Hydrogen in Disordered and Amorphous Solids* ed G Bambakidis and R C Bowman (Springer US) pp 81–90
[17] Hansen U and Vogl P 1998 Hydrogen passivation of silicon surfaces: a classical molecular-dynamics study *Phys. Rev. B* **57** 13295–304
[18] Lee S H, Bhopal M F, Lee D W and Lee S H 2018 Review of advanced hydrogen passivation for high efficient crystalline silicon solar cells *Mater. Sci. Semicond. Process.* **79** 66–73
[19] Madi D, Prathap P and Slaoui A 2015 Role of MW-ECR hydrogen plasma on dopant deactivation and open-circuit voltage in crystalline silicon solar cells *Appl. Phys. A* **118** 231–7
[20] Zhang Z, Sun Q, Lu Y, Lu F, Mu X, Wei S-H and Sui M 2022 Hydrogenated $Cs_2AgBiBr_6$ for significantly improved efficiency of lead-free inorganic double perovskite solar cell *Nat. Commun.* **13** 3397
[21] Coutinho J, Gomes D, Torres V J B, Fattah T O A, Markevich V P and Peaker A R 2024 Hydrogen reactions with dopants and impurities in solar silicon from first principles *Sol. RRL* **8** 2300639
[22] Dopilka A, Childs A, Bobev S and Chan C K 2021 Electrochemical lithium alloying behavior of guest-free Type II silicon clathrates *J. Phys. Chem. C* **125** 19110–8
[23] Liu Y, Briggs J P, Majid A A A, Furtak T E, Walker M, Singh M, Koh C A, Taylor P C and Collins R T 2023 Formation of Type II silicon clathrate with lithium guests through thermal diffusion *Inorg. Chem.* **62** 6882–92
[24] Krishna L and Koh C A 2015 Inorganic and methane clathrates: versatility of guest–host compounds for energy harvesting *MRS Energy Sustain.* **2** 8
[25] Cousins K and Zhang R 2019 Highly porous organic polymers for hydrogen fuel storage *Polymers* **11** 690
[26] Djokic M and Mendoza-Cortes J L 2024 MultiBinding sites united in covalent-organic frameworks (MSUCOF) for H_2 storage and delivery at room temperature *Energy Fuels* **38** 4711–20
[27] Chen Z, Kirlikovali K O, Idrees K B, Wasson M C and Farha O K 2022 Porous materials for hydrogen storage *Chem* **8** 693–716
[28] Bharwal A K *et al* 2025 Enhancing morphological and optoelectronic properties of silicon clathrate films through thermal press annealing and SF_6 treatment *ACS Appl. Energy Mater.* **8** 1752–8
[29] Slaoui A, Pihan E, Ka I, Mbow N A, Roques S and Koebel J M 2006 Passivation and etching of fine-grained polycrystalline silicon films by hydrogen treatment *Sol. Energy Mater. Sol. Cells* **90** 2087–98
[30] Bharwal A K *et al* 2024 Comparative energy levels analysis of Type I and Type II silicon clathrate films *MRS Adv.* **9** 1685–90
[31] Guyot Y, Champagnon B, Reny E, Cros C, Pouchard M, Melinon P, Perez A and Gregora I 1998 Raman scattering of silicon clathrates *Phys. Rev. B* **57** R9475–7
[32] Grey L H, Nie H-Y and Biesinger M C 2024 Defining the nature of adventitious carbon and improving its merit as a charge correction reference for XPS *Appl. Surf. Sci.* **653** 159319
[33] Stoquert J P, Pêcheux F, Hervé Y, Marchal H, Stuck R and Siffert P 1998 VRBS: a virtual RBS simulation tool for ion beam analysis *Nucl. Instrum. Methods Phys. Res. B* **136–138** 1152–6